A NUMERICAL STUDY ON HEATING PERFORMANCE OF HORIZONTAL AND VERTICAL EARTH-AIR HEAT EXCHANGERS WITH EQUAL PIPE LENGTHS

by

Fatih TASDELEN[a*] and Ihsan DAGTEKIN[b]

[a] Technical Sciences Vocational School, Bitlis Eren University, Bitlis, Turkey
[b] Department of Mechanical Engineering, Fırat University, Elazig, Turkey

Original scientific paper
https://doi.org/10.2298/TSCI2204929T

In this study, heating performances of horizontal and vertical earth-air heat exchangers with equal pipe lengths were evaluated in ANSYS FLUENT 19.2 simulation program based on CFD for the winter period of Bitlis, Turkey. Thermal performance analyses regarding vertical and horizontal 3-D-modeled earth-air heat exchangers were evaluated in steady-state condition of the simulation program for different values of Re = $5\cdot10^3$, 10^4, $2\cdot10^4$, $4\cdot10^4$, $6\cdot10^4$, $8\cdot10^4$, and 10^5 numbers by using standard k-ε turbulence model. Numerical results obtained from CFD based simulation program were compared with a numerical study in the literature, and it was determined that there was a consistency between the results. The pressure loss and fan power values of horizontal and vertical earth-air heat exchangers were also investigated in addition their thermal performances. A good agreement was found between the pressure loss values obtained from the theoretical and simulation calculations of both earth-air heat exchangers. Considering the temperature increases in both earth-air heat exchangers, the highest and lowest temperature increases were observed in vertical earth-air heat exchanger with 22.52 K and 10.67 K, respectively. The best thermal performance was observed in vertical earth-air heat exchanger for $5\cdot10^3$, 10^4, and $2\cdot10^4$ values of Reynolds number and in horizontal earth-air heat exchanger for $4\cdot10^4$, $6\cdot10^4$, $8\cdot10^4$, and 10^5 values of Reynolds number.

Key words: *earth-air heat exchanger, CFD, temperature, Reynolds number, earth, thermal performance*

Introduction

Global primary energy demand is increasing day by day, and approximately one-third of the total energy demand is essential for space heating and cooling. Therefore, most of the countries have directed towards passive and low grade energy systems to meet their heating and cooling needs [1]. Earth-air heat exchangers (EAHE) can be given as a good example for these energy systems. The EAHE systems are used to improve thermal conditions of buildings with less energy by utilizing the heat of the earth. Many researchers have carried out various studies regarding EAHE systems. For example, Kaushal [2] investigated the effect of parameters such as pipe material, earth thermal conductivity and air velocity on the thermal performance of EAHE. Cao *et al.* [3] examined the applicability of EAHE in a building through theoretical calculation and numerical simulation. Soares *et al.* [4] presented systematic information regard-

* Corresponding author, e-mail: ftasdelen@beu.edu.tr

ing the main design parameters and operating conditions affecting the overall performance of EAHE. Yang *et al.* [5] found that a cooling or heating capacity of 3000 W could be achieved with the use of an EAHE pipe. Bansal *et al.* [6] analyzed the effect of thermal conductivity of the earth surrounding the EAHE pipe and operating time of EAHE on its thermal performance. Mathur *et al.* [7] conducted design, development and experimental studies to analyze the thermal performance of straight and spiral EAHE system. Singh *et al.* [8] investigated the latest developments regarding EAHE, its modelling and design process, the effects of different design and operating parameters on thermal performance of the system and its installation schemes. Serageldin *et al.* [9] examined the thermal performance of an EAHE used for heating and cooling by using CFD simulation and mathematical model as well as experimental study. Bansal *et al.* [10] found that the pipe material did not significantly affect the performance of EAHE. Wei *et al.* [11] analyzed the cooling capacities of EAHE in a hot and humid climate. Ozgener and Ozgener [12] investigated the performance properties of a galvanized earth heat exchanger with 47 m horizontal and 56 cm nominal diameter. Esen *et al.* [13] investigated the energetic and exergetic efficiency of a ground-coupled heat pump system for the heating season. Al-Ajmi *et al.* [14] developed a theoretical model to predict the cooling potential and outlet air temperature of an EAHE under hot and arid climate conditions. Ozgener and Ozgener [15] evaluated the performance of EAHE system for greenhouse heating. Ozgener and Ozgener [16] examined thermo-economic parameters of a prototype EAHE system. Ahmed *et al.* [17] found that the performance of EAHE varied by the size of the examined area and climate.

In this study, thermal performances of horizontal and vertical 3-D-modeled EAHE systems were investigated by using CFD-based package software. Unlike studies in the literature, pipe lengths of horizontal and vertical EAHE systems were modeled equally. In this context, as a result of the simulations, which of horizontal and vertical EAHE systems is more advantageous to use for passive heating will be determined. Thermal performance analyses regarding vertical and horizontal EAHEs were evaluated in steady-state condition of the simulation program for different values of Re = $5\cdot10^3$, 10^4, $2\cdot10^4$, $4\cdot10^4$, $6\cdot10^4$, $8\cdot10^4$, and 10^5 numbers by using standard k-ε turbulence model.

Information regarding earth-air heat exchangers

Schematic drawings of horizontal and vertical EAHE designed for winter season heating of a building in Bitlis, Turkey, are given in figs. 1 and 2.

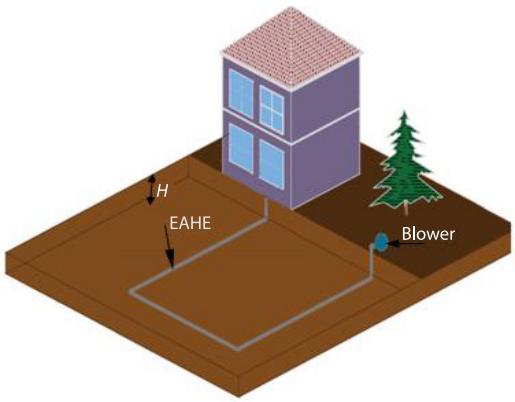

Figure 1. Schematic drawing of horizontal EAHE

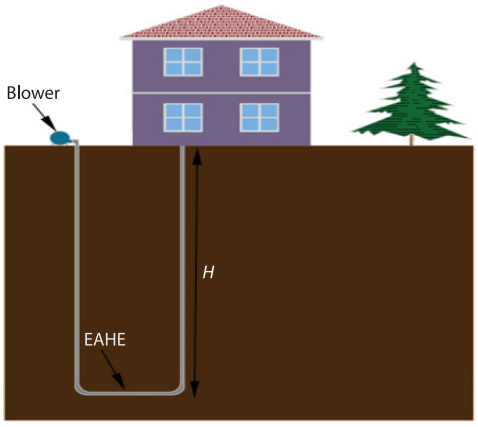

Figure 2. Schematic drawing of vertical EAHE

Pipe length, pipe inner diameter and pipe wall thickness of both EAHE were 30.64 m, 0.05 m, and 0.004 m, respectively. The horizontal EAHE shown in fig. 1 was buried at $H = 1$ m depth, while the vertical EAHE shown in fig. 2 was buried at $H = 13.482$ m depth. Pipe material of both EAHE was preferred as PVC.

Methods

Model equations

Continuity, eq. (1), Navier-Stokes, eqs. (2a)-(2c), and energy equations, eq. (3), for heat, mass transfer and fluid-flow in 3-dimensional cylindrical co-ordinates can be written [18]:

$$\frac{1}{r}\frac{\partial\left(ru_r\right)}{\partial r}+\frac{1}{r}\frac{\partial u_\theta}{\partial\theta}+\frac{\partial u_z}{\partial z}=0 \tag{1}$$

$$\rho\left(\frac{\partial u_r}{\partial t}+u_r\frac{\partial u_r}{\partial r}+\frac{u_\theta}{r}\frac{\partial u_r}{\partial\theta}+u_z\frac{\partial u_r}{\partial z}-\frac{u_\theta^2}{r}\right)=$$

$$=\rho g_r-\frac{\partial p}{\partial r}+\mu\left[\frac{1}{r}\frac{\partial}{\partial r}\left(r\frac{\partial u_r}{\partial r}\right)+\frac{1}{r^2}\frac{\partial^2 u_r}{\partial\theta^2}+\frac{\partial^2 u_r}{\partial z^2}-\frac{2}{r^2}\frac{\partial u_\theta}{\partial\theta}-\frac{u_r}{r^2}\right] \tag{2a}$$

$$\rho\left(\frac{\partial u_\theta}{\partial t}+u_r\frac{\partial u_\theta}{\partial r}+\frac{u_\theta}{r}\frac{\partial u_\theta}{\partial\theta}+u_z\frac{\partial u_\theta}{\partial z}+\frac{u_r u_\theta}{r}\right)=$$

$$=\rho g_\theta-\frac{1}{r}\frac{\partial p}{\partial\theta}+\mu\left[\frac{1}{r}\frac{\partial}{\partial r}\left(r\frac{\partial u_\theta}{\partial r}\right)+\frac{1}{r^2}\frac{\partial^2 u_\theta}{\partial\theta^2}+\frac{\partial^2 u_\theta}{\partial z^2}+\frac{2}{r^2}\frac{\partial u_r}{\partial\theta}-\frac{u_\theta}{r^2}\right] \tag{2b}$$

$$\rho\left(\frac{\partial u_z}{\partial t}+u_r\frac{\partial u_z}{\partial r}+\frac{u_\theta}{r}\frac{\partial u_z}{\partial\theta}+u_z\frac{\partial u_z}{\partial z}\right)=\rho g_z-\frac{\partial p}{\partial z}+\mu\left[\frac{1}{r}\frac{\partial}{\partial r}\left(r\frac{\partial u_z}{\partial r}\right)+\frac{1}{r^2}\frac{\partial^2 u_z}{\partial\theta^2}+\frac{\partial^2 u_z}{\partial z^2}\right] \tag{2c}$$

$$\frac{\partial T}{\partial t}+u_r\frac{\partial T}{\partial r}+\frac{u_\theta}{r}\frac{\partial T}{\partial\theta}+u_z\frac{\partial T}{\partial z}=\frac{\dot{q}_g}{c_p}+\alpha\left[\frac{1}{r}\frac{\partial}{\partial r}\left(r\frac{\partial T}{\partial r}\right)+\frac{1}{r^2}\frac{\partial^2 T}{\partial\theta^2}+\frac{\partial^2 T}{\partial z^2}\right]+\frac{\Phi}{\rho c_p} \tag{3}$$

The viscous distribution ratio in the energy equation can be written:

$$\Phi=2\mu\left[\left(\frac{\partial u_r}{\partial r}\right)^2+\left(\frac{1}{r}\frac{\partial u_\theta}{\partial\theta}+\frac{u_r}{r}\right)^2+\left(\frac{\partial u_z}{\partial z}\right)^2\right]+$$

$$\mu\left[\left(\frac{1}{r}\frac{\partial u_r}{\partial\theta}+\frac{\partial u_\theta}{\partial r}-\frac{u_\theta}{r}\right)^2+\left(\frac{\partial u_\theta}{\partial z}+\frac{1}{r}\frac{\partial u_z}{\partial\theta}\right)^2+\left(\frac{\partial u_z}{\partial r}+\frac{\partial u_r}{\partial z}\right)^2\right] \tag{4}$$

In terms of accuracy and convergence robustness in the solution of the designed models, standard k-ε turbulence model will be used for numerical analyses to be conducted since k-ε turbulence model will be a good choice for this purpose. Turbulence kinetic energy, k, and turbulence spreading rate, ε, are obtained [19]:

$$\frac{\partial}{\partial t}\left(\rho k\right)+\frac{\partial}{\partial x_i}\left(\rho k u_i\right)=\frac{\partial}{\partial x_j}\left[\left(\mu+\frac{\mu_t}{\sigma_k}\right)\frac{\partial k}{\partial x_j}\right]+G_k+G_b-\rho\varepsilon-Y_M+S_k \tag{5}$$

$$\frac{\partial}{\partial t}\left(\rho\varepsilon\right)+\frac{\partial}{\partial x_i}\left(\rho\varepsilon u_i\right)=\frac{\partial}{\partial x_j}\left[\left(\mu+\frac{\mu_t}{\sigma_\varepsilon}\right)\frac{\partial\varepsilon}{\partial x_j}\right]+C_{1\varepsilon}\frac{\varepsilon}{k}\left(G_k+C_{3\varepsilon}G_b\right)-C_{2\varepsilon}\rho\frac{\varepsilon^2}{k}+S_\varepsilon \tag{6}$$

where G_b is the generation of turbulence kinetic energy due to buoyancy, G_k – the generation of turbulence kinetic energy due to average velocity gradients, and Y_M – the contribution of fluctuating dilatation in compressible turbulence to the overall dissipation rate. The $C_{1\varepsilon}$, $C_{2\varepsilon}$, and $C_{3\varepsilon}$ are constants and σ_k and σ_ε – the turbulence Prandtl numbers for k and ε, respectively. The S_k and S_ε refer to user-defined source terms. Turbulent viscosity is calculated with the combination of μ_t, k, and ε [19]:

$$\mu_t = \rho C_\mu \frac{k^2}{\varepsilon} \tag{7}$$

where $C_{1\varepsilon}$, $C_{2\varepsilon}$, C_μ, σ_k, and σ_ε are model constants and have the default values [19]:

$$C_{1\varepsilon} = 1.44,\ C_{2\varepsilon} = 1.92,\ C_\mu = 0.09,\ \sigma_k = 1.0,\ \sigma_\varepsilon = 1.3$$

These default values were obtained from experimental data for basic turbulent flows with frequently encountered shear flows such as boundary-layers mixed layers, and jets [19].

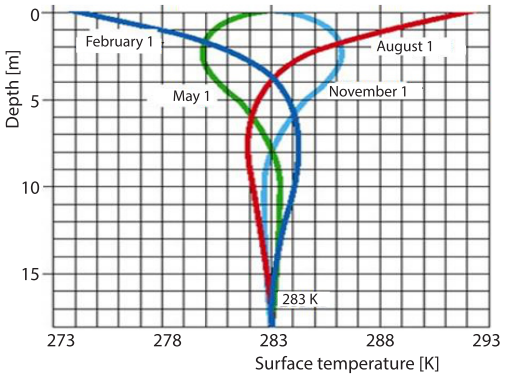

Figure 3. Change of Earth temperature [21]

Boundary and initial conditions

Prior to the numerical simulations, the boundary and initial conditions must be entered in the program. The temperature values regarding 1 m depth of earth and outdoor air to be used for the thermal analysis of both EAHE were obtained from Bitlis Provincial Directorate of Meteorology (data of February 2019) [20]. In all numerical analyses, 257.30 K, which was the minimum air temperature value of February 2019 of Bitlis, Turkey, was used as the air inlet temperature. Horizontal EAHE was buried at H = 1 m depth of earth and the average earth temperature at this depth is 277 K. For this reason, pipe surface temperature value of horizontal EAHE was accepted as 277 K in all numerical analyses. Vertical EAHE was buried at H = 13.482 m depth of earth. Since the earth temperature values of the aforementioned depth, at which vertical EAHE was buried, were not available in the Provincial Directorate of Meteorology, the graph in fig. 3 was used to determine the average earth temperature values of this depth.

Thermal conductivity of the earth in all numerical analyses was accepted as k_e = 0.52 W/mK. The physical and thermal properties of the materials used in a package software are given in tab. 1.

Comparison with literature

Results obtained from CFD-based package software were compared with a numerical study conducted by Misra *et al.* [22] and it was determined that there was a consistency between the results. The numerical study of Misra *et al.* [22] was analyzed by using the standard k-ε turbulence model in steady-state condition of the package software. The physical and thermal properties of the numerical model of Misra *et al.* [22] are presented in tab. 2.

The results of the CFD simulation and numerical study of Misra *et al.* [22] are presented in tab. 3 and fig. 4. When tab. 3 and fig. 4 are examined, it is seen that there is a consistency between the results of CFD simulation and numerical study of Misra *et al.* [22]. Therefore, it

was determined that very sensitive and accurate results would be obtained with CFD-based package software simulation program by using the standard k-ε turbulence model.

Table 1. Physical and thermal properties of the materials used in the simulation

Parameters	Values
EAHE length [m]	30.64
Pipe inner diameter [m]	0.05
Pipe wall thickness [m]	0.004
Temperature of air at EAHE inlet [K]	257.30
Density of air [kgm^{-3}]	1.371
Thermal conductivity of air [Wm^{-1}K^{-1}]	0.0224
Dynamic viscosity of air [kgm^{-1}s^{-1}]	$1.651 \cdot 10^{-5}$
Specific heat capacity of air [Jkg^{-1}K^{-1}]	1005.43
Thermal conductivity of earth [Wm^{-1}K^{-1}]	0.52
Density of earth [kgm^{-3}]	2050
Specific heat capacity of earth [Jkg^{-1}K^{-1}]	1840
Thermal conductivity of PVC [Wm^{-1}K^{-1}]	0.16
Density of PVC [kgm^{-3}]	1380
Specific heat capacity of PVC [Jkg^{-1}K^{-1}]	900

Table 2. Physical and thermal properties of the numerical model of [22]

Parameters	Values
Temperature of air at EAHE inlet [K]	280.6
Air velocity [ms^{-1}]	5
Density of air [kgm^{-3}]	1.225
Thermal conductivity of air [Wm^{-1}K^{-1}]	0.0242
Specific heat capacity of air [Jkg^{-1}K^{-1}]	1006
Earth temperature [K]	300.2
Thermal conductivity of earth [Wm^{-1}K^{-1}]	4
Density of earth [kgm^{-3}]	2050
Specific heat capacity of earth [Jkg^{-1}K^{-1}]	1840
Thermal conductivity of PVC [Wm^{-1}K^{-1}]	1.16
Density of PVC [kgm^{-3}]	1380
Specific heat capacity of PVC [Jkg^{-1}K^{-1}]	900

Table 3. Air temperatures for CFD simulation and [22] numerical model [K]

Pipe length [m]	[22]	CFD simulation	Relative error [%]
0	280.60	280.60	0
5	287.30	289.28	0.69
10	292.90	294.15	0.43
15	296	296.85	0.29
20	297.80	298.33	0.18
30	299.50	299.62	0.04
40	300	300.03	0.01
50	300.20	300.15	0.02
60	300.20	300.18	0.01

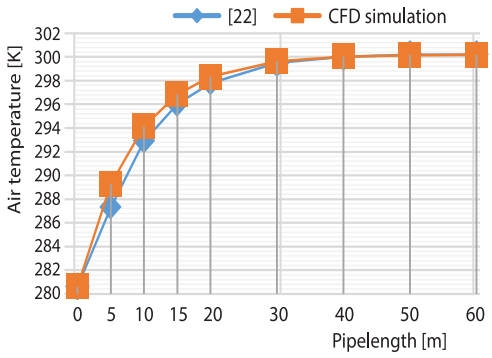

Figure 4. Validation of CFD results with study conducted by [22]

Evaluation of simulation results

Heating performances of horizontal and vertical EAHE with equal pipe lengths were analyzed by using different values of Re = $5\cdot10^3$, 10^4, $2\cdot10^4$, $4\cdot10^4$, $6\cdot10^4$, $8\cdot10^4$, 10^5 numbers and standard k-ε turbulence model in CFD-based package software. Pressure losses and fan power values of both EAHE, whose heating performances were investigated, were also examined. After pressure loss values of horizontal and vertical EAHE were calculated theoretically, they were compared with pressure loss values obtained from simulation program.

Examination of pressure loss and fan power values

Pressure loss values, ΔP, of vertical and horizontal EAHE can be expressed [23]:

$$\Delta P = 0.5 f \frac{L}{D} \rho U^2 + \Delta\zeta \tag{8}$$

where ρ is the fluid density, U – the fluid velocity, f – the Darcy friction factor, and ζ – the specific resistance losses through pipe and L pipe length. Pressure loss values of horizontal and vertical EAHE according to the theoretical and CFD simulation calculations are presented in tab. 4. When tab. 4 is examined, it is seen that there is a consistency between pressure loss values of EAHE according to the theoretical and CFD simulation calculations. In line with these results, it was determined that accurate results could be obtained with the package software by using standard k-ε turbulence model in terms of flows in pipe. After calculating pressure losses of both EAHE, selection of an appropriate fan is highly important in terms of enabling air circulation. Fan power value can be [24]:

$$\dot{E}_{\text{fan}} = \frac{\left(\frac{\dot{m}_{\text{a}}}{\rho}\right)\Delta P}{\eta_{\text{fan}}} \tag{9}$$

where ΔP is the pressure loss value obtained from CFD simulation results and η_{fan} – the fan efficiency value. To provide air circulation in PVC pipes radial-type fan widely used in air handling units and industry was selected and radial fan efficiency was accepted as 0.85. Fan power values of both EAHE are given in tab. 5.

Table 4. Pressure loss values for theoretical and CFD simulation

EAHE	H-EAHE		V-EAHE	
	Theoretical results	CFD results	Theoretical results	CFD results
Reynolds number	ΔP [Pa]	ΔP [Pa]	ΔP [Pa]	ΔP [Pa]
5000	24.71	23.35	24.11	23.05
10000	81.45	76.95	79.06	76.20
20000	273.87	258.72	264.33	255.24
40000	936.40	883.08	898.24	871.93
60000	1935.13	1819.29	1849.27	1791.89
80000	3247.54	3043.76	3094.91	3009.19
100000	4859.45	4549.28	4620.96	4489.57

Table 5. Fan power values

EAHE	H-EAHE	V-EAHE
Reynolds number	$\dot{E}_{\text{fan}}$ [W]	$\dot{E}_{\text{fan}}$ [W]
5000	0.065	0.064
10000	0.428	0.424
20000	2.864	2.825
40000	19.627	19.379
60000	60.573	59.660
80000	135.296	133.759
100000	252.965	249.645

Heating performance of horizontal EAHE

The air entering in the horizontal EAHE at a temperature of 257.30 K left the pipe at 276.89 K and 268.83 K in $5 \cdot 10^3$ and 10^5 values of Reynolds number, respectively. Table 6 shows the average air temperature values obtained through EAHE length for different values of Reynolds number.

Table 6. Average air temperatures along the length of horizontal EAHE

Reynolds number	$5 \cdot 10^3$	10^4	$2 \cdot 10^4$	$4 \cdot 10^4$	$6 \cdot 10^4$	$8 \cdot 10^4$	10^5
Pipe length [m]	Average air temperature [K]						
0	257.30	257.30	257.30	257.30	257.30	257.30	257.30
6	275.76	273.40	269.10	264.68	262.75	261.59	260.84
12	276.73	275.88	273.07	268.55	265.99	264.38	263.22
18	276.90	276.57	274.95	271.18	268.50	266.66	265.32
24	276.93	276.78	275.86	272.86	270.35	268.44	266.98
30.64	276.89	276.79	276.33	274.29	272.14	270.33	268.83

When tab. 6 is examined, it is seen that there is a temperature difference of 8.06 K between the average air temperature values obtained for the highest and lowest values of Reynolds number at pipe outlet. The reason for this is that the average air velocity value in the pipe is lower at the lowest value of Reynolds number. As the average air velocity value decreases, cold air in the pipe becomes warmer. When tab. 6 is examined, it is seen that the average air temperature values in the pipe decrease as the value of Reynolds number increases. The average air temperature increases at different distances of horizontal EAHE are given in tab. 7.

Table 7. Average air temperature rises along the length of horizontal EAHE

Reynolds number	$5 \cdot 10^3$	10^4	$2 \cdot 10^4$	$4 \cdot 10^4$	$6 \cdot 10^4$	$8 \cdot 10^4$	10^5
Pipe length [m]	Average air temperature rise [K]						
0-6	18.46	16.10	11.80	7.38	5.45	4.29	3.54
0-12	19.43	18.58	15.77	11.25	8.69	7.08	5.92
0-18	19.60	19.27	17.65	13.88	11.20	9.36	8.02
0-24	19.63	19.48	18.56	15.56	13.05	11.14	9.68
0-30.64	19.59	19.49	19.03	16.99	14.84	13.03	11.53

When tab. 7 is examined, it is seen that temperature increases of 19.59 K and 11.53 K occurred for $5 \cdot 10^3$ and 10^5 values of Reynolds number at pipe outlets. Moreover, as the value of Reynolds number increased, the average air temperature increases through the pipe also decreased. Earth, pipe and air-related temperature contours in horizontal EAHE system for $5 \cdot 10^3$ and 10^5 values of Reynolds number are given in figs. 5 and 6.

Since the air-flow velocity in pipe will increase due to the increase in Reynolds number, the cold air will leave the pipe faster and the air in pipe will warm less. When figs. 5 and Fig. 6 are examined, it is seen that the cold air in the pipe approached the earth temperature for $5 \cdot 10^3$ value of Reynolds number, however, it decreased earth temperature for 10^5 value. As a result, it was determined that thermal performance in pipe decreased due to the increase in Reynolds number.

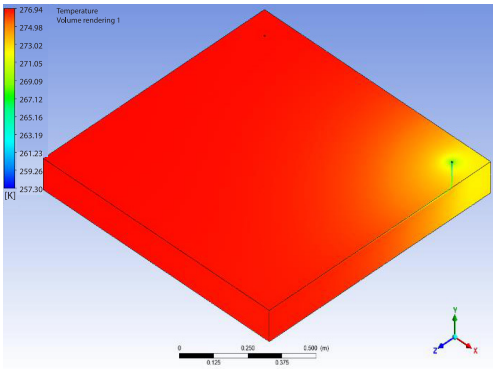

Figure 5. Temperature contours of earth, pipe and air (Re = $5 \cdot 10^3$)

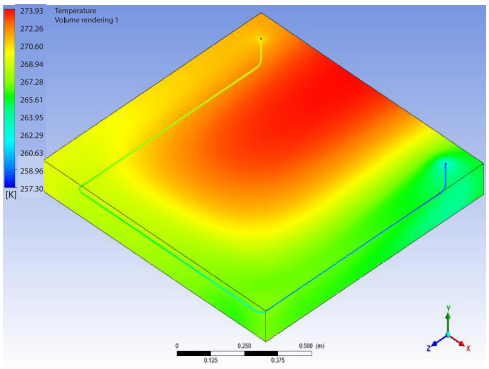

Figure 6. Temperature contours of earth, pipe and air (Re = 10^5)

Heating performance of vertical EAHE

The air entering in vertical EAHE at temperature of 257.30 K was found to be, respectively 279.82 K and 267.97 K at pipe outlet for $5 \cdot 10^3$ and 10^5 values of Reynolds number. The average air temperature values obtained for different values of Reynolds number through the vertical EAHE length are presented in tab. 8.

Table 8. Average air temperatures along the length of vertical EAHE

Reynolds number	$5 \cdot 10^3$	10^4	$2 \cdot 10^4$	$4 \cdot 10^4$	$6 \cdot 10^4$	$8 \cdot 10^4$	10^5
Pipe length [m]	Average air temperature [K]						
0	257.30	257.30	257.30	257.30	257.30	257.30	257.30
6	279.94	276.87	271.24	265.82	263.23	261.79	260.87
12	281.37	280.13	276.35	270.54	267.10	264.96	263.55
18	281.55	280.81	278.19	273.02	269.50	267.08	265.42
24	281.09	280.30	278.33	274.13	270.90	268.56	266.86
30.64	279.82	278.61	277.10	274.16	271.58	269.55	267.97

When tab. 8 is examined, it is seen that as the value of Reynolds number increases, the average air temperature values through vertical EAHE length decrease like in horizontal EAHE and there is a temperature difference of 11.85 K between the average air temperature values obtained for the highest and lowest values of Reynolds number at pipe outlet. In horizontal EAHE, this temperature difference was 8.06 K. It has been determined that the difference between the average air temperature values observed at the pipe outlet for the highest and lowest values of the Reynolds number is greater in the vertical EAHE. The average air temperature increases at different distances of vertical EAHE are given in tab. 9.

Table 9. Average air temperature rises along the length of vertical EAHE

Reynolds number	$5 \cdot 10^3$	10^4	$2 \cdot 10^4$	$4 \cdot 10^4$	$6 \cdot 10^4$	$8 \cdot 10^4$	10^5
Pipe length [m]	Average air temperature rise [K]						
0-6	22.64	19.57	13.94	8.52	5.93	4.49	3.57
0-12	24.07	22.83	19.05	13.24	9.80	7.66	6.25
0-18	24.25	23.51	20.89	15.72	12.20	9.78	8.12
0-24	23.79	23	21.03	16.83	13.60	11.26	9.56
0-30.64	22.52	21.31	19.80	16.86	14.28	12.25	10.67

When tab. 9 is examined, it is seen that average air temperature increases of 22.52 K and 10.67 were observed for $5 \cdot 10^3$ and 10^5 values of Reynolds number at pipe outlets. When tabs. 7 and 9 are examined, it is seen that the average air temperature increases at vertical EAHE outlet for $5 \cdot 10^3$, 10^4, and $2 \cdot 10^4$ values of Reynolds number are higher than the average air temperature increases at horizontal EAHE outlet. Despite these results, the average air temperature increases at horizontal EAHE for $4 \cdot 10^4$, $6 \cdot 10^4$, $8 \cdot 10^4$, and 10^5 values of Reynolds number were higher than the average air temperature increases at vertical EAHE outlet. Earth, pipe and air-related temperature contours in vertical EAHE system for $5 \cdot 10^3$ and 10^5 values of Reynolds number are given in figs. 7 and 8.

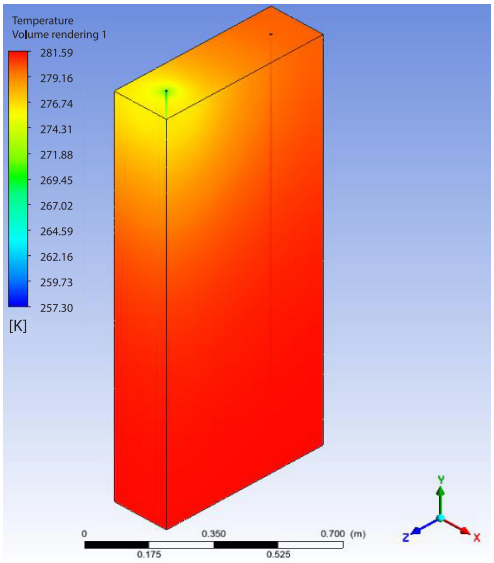

Figure 7. Temperature contours of earth pipe and air (Re = $5 \cdot 10^3$)

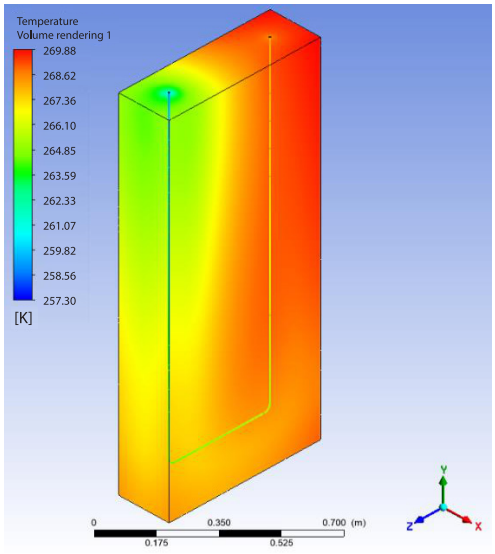

Figure 8. Temperature contours of earth pipe and air (Re = 10^5)

Figures 7 and 8 reveal that the cold air in the pipe approached the earth temperature in $5 \cdot 10^3$ value of Reynolds number like in horizontal EAHE and the cold air in the pipe decreased earth temperature in 10^5 value of Reynolds number. It was determined that thermal performances in pipe decreased due to the increase in Re number in vertical EAHE like in horizontal EAHE.

Conclusions

Heating performances of horizontal and vertical EAHE with equal pipe lengths were investigated by using air and earth temperature data of Bitlis, Turkey, in February 2019. The CFD-based package software simulation program was used to evaluate the heating performances of horizontal and vertical EAHE. Numerical simulations were carried out for the average air-flow velocities obtained from different values of Re = $5 \cdot 10^3$, 10^4, $2 \cdot 10^4$, $4 \cdot 10^4$, $6 \cdot 10^4$, $8 \cdot 10^4$, and 10^5 numbers by using standard k-ε turbulence model. The results obtained from CFD-based simulation program are summarized are as follows.

- It has been determined that the pressure loss values obtained from the theoretical and CFD simulations of both EAHE increased through pipe length depending on the increase in Reynolds number. The lowest pressure loss value obtained from CFD simulations was ob-

served in vertical EAHE with 23.05 Pa, while the highest pressure loss value was detected in horizontal EAHE with 4549.28 Pa.

- Fan power values of horizontal EAHE were found to be 0.065 W and 252.965 W for $5 \cdot 10^3$ and 10^5 values of Reynolds number. These values were 0.064 W and 249.645 W for vertical EAHE.
- The best thermal performance of both EAHE was observed in $5 \cdot 10^3$ value of Reynolds number, while the worst thermal performance was seen in 10^5 value.
- Considering the temperature increases in both EAHE, the highest and lowest temperature increases were observed in vertical EAHE with 22.52 K and 10.67 K, respectively.
- The best thermal performances were observed in vertical EAHE for $5 \cdot 10^3$, 10^4, and $2 \cdot 10^4$ values of Reynolds number and in horizontal EAHE for $4 \cdot 10^4$, $6 \cdot 10^4$, $8 \cdot 10^4$, and 10^5 values of Reynolds number.

Finally, it has been determined that vertical EAHE should be preferred for $5 \cdot 10^3$, 10^4, and $2 \cdot 10^4$ values of Reynolds number and horizontal EAHE should be preferred for $4 \cdot 10^4$, $6 \cdot 10^4$, $8 \cdot 10^4$, and 10^5 values of Reynolds number for passive heating in winter season of a building in Bitlis, Turkey.

Acknowledgment

This study is produced from the Ph. D. thesis study of F. Tasdelen.

Nomenclature

c_p – specific heat, [Jkg^{-1}K^{-1}]
D – pipe inner diameter, [m]
f – Darcy friction factor
g – gravitational acceleration, [ms^{-2}]
H – buried pipe depth, [m]
k – thermal conductivity, [Wm^{-1}K^{-1}]
L – pipe length, [m]
$\dot{m}$ – mass-flow rate, [kgs^{-1}]
ΔP – pressure loss, [Pa]
p – pressure, [Pa]
Re – Reynolds number
r, θ, z – cylindrical co-ordinate variables
T – temperature, [K]
U – fluid velocity, [ms^{-1}]

Greek symbols

μ – viscosity, [kgm^{-1}s^{-1}]
ρ – density, [kgm^{-3}]
Φ – viscous distribution ratio

Subscripts

a – air
e – earth
t – turbulence

Acronyms

EAHE – earth-air heat exchanger
PVC – polyvinyl chloride

References

[1] Agrawal, K. K., et al., Experimental Study to Investigate the Effect of Water Impregnation on Thermal Performance of Earth Air Tunnel Heat Exchanger for Summer Cooling in Hot and Arid Climate, *Renewable Energy*, *120* (2018), May, pp. 255-265
[2] Kaushal, M., Performance Analysis of Clean Energy Using Geothermal Earth to Air Heat Exchanger (GEAHE) in Lower Himalayan Region – Case Study Scenario, *Energy and Buildings*, *248* (2021) Oct., 111166
[3] Cao, S., *et al*., Feasibility Analysis of Earth-Air Heat Exchanger (EAHE) in A Sports and Culture Center in Tianjin, China, *Case Studies in Thermal Engineering*, *26* (2021), 101054
[4] Soares, N., *et al*., Advances in Standalone and Hybrid Earth-Air Heat Exchanger (EAHE) Systems for Buildings: *A Review, Energy and Buildings*, *253* (2021), 111532
[5] Yang, D., *et al*., Evaluation of the Thermal Performance of an Earth-to-Air Heat Exchanger (EAHE) in a Harmonic Thermal Environment, *Energy Conversion and Management*, *109* (2016), Feb., pp. 184-194
[6] Bansal, V., *et al*., Derating Factor New Concept for Evaluating Thermal Performance of Earth Air Tunnel Heat Exchanger: A Transient CFD Analysis, *Applied Energy*, *102* (2013), Feb., pp. 418-426
[7] Mathur, A., *et al*., Comparative Study of Straight and Spiral Earth Air Tunnel Heat Exchanger System Operated in Cooling and Heating Modes, *Renewable Energy*, *108* (2017), Aug., pp. 474-487

[8] Singh, R., *et al*., Recent Advancements in Earth Air Tunnel Heat Exchanger (EATHE) System for Indoor Thermal Comfort Application: *A Review, Renewable and Sustainable Energy Reviews*, *82* (2018), Feb., pp. 2162-2185
[9] Serageldin, A. A., *et al*., Earth-Air Heat Exchanger Thermal Performance in Egyptian Conditions: Experimental Results, Mathematical Model, and Computational Fluid Dynamics Simulation, *Energy Conversion and Management*, *122* (2016), Aug., pp. 25-38
[10] Bansal, V., *et al*., Performance Analysis of Earth-Pipe-Air Heat Exchanger for Winter Heating, *Energy and Buildings*, *41* (2009), 11, pp. 1151-1154
[11] Wei, H., *et al*., Field Experiments on the Cooling Capability of Earth-to-Air Heat Exchangers in Hot and Humid Climate, *Applied Energy*, *276* (2020), 115493
[12] Ozgener, L., Ozgener, O., Energetic Performance Test of an Underground Air Tunnel System for Greenhouse Heating, *Energy*, *35* (2010), 10, pp. 4079-4085
[13] Esen, H., *et al*., Energy and Exergy Analysis of a Ground-Coupled Heat Pump System with Two Horizontal Ground Heat Exchangers, *Building and Environment*, *42* (2007), 10, pp. 3606-3615
[14] Al-Ajmi, F., *et al.*, The Cooling Potential of Earth-Air Heat Exchangers for Domestic Buildings in a Desert Climate, *Building and Environment*, *41* (2006), 3, pp. 235-244
[15] Ozgener, O., Ozgener, L., Determining the Optimal Design of a Closed Loop Earth to Air Heat Exchanger for Greenhouse Heating by Using Exergoeconomics, *Energy and Buildings*, *43* (2011), 4, pp. 960-965
[16] Ozgener, L., Ozgener, O., Three Heating Seasons Monitoring of Thermo-Economic Parameters of a Prototype EAHE System for Technological Forecasting and Evaluating Low Grade Geothermal Resources in Turkey, *Energy and Buildings*, *66* (2013), Nov., pp. 346-352
[17] Ahmed, A., *et al*., Thermal Performance of Earth-Air Heat Exchanger for Reducing Cooling Energy Demand of Office Buildings in The United Kingdom, *Proceedings*, 11th Conference of International Building Performance Simulation Association, Glasgow, Scotland, 2009, pp. 2228-2235
[18] Salih, A., *Conservation Equations of Fluid Dynamics, Department of Aerospace Engineering*, Indian Institute of Space Science and Technology, Thiruvananthapuram, India, 2011
[19] ***, ANSYS Fluent Theory Guide, Release 2020 R1, http://www.ansys.com
[20] ***, Bitlis Meteorology Provincial Directorate, httpss://www.mgm.gov.tr
[21] ***, Change of Earth Temperature, https://www.slideshare.net/guest2bda06/tkip
[22] Misra, R., *et al*., Transient Analysis Based Determination of Derating Factor for Earth Air Tunnel Heat Exchanger in Winter, *Energy and Buildings*, *58* (2013), Mar., pp. 76-85
[23] Ozgener, L., Ozgener, O., An Experimental Study of the Exergetic Performance of an Underground Air Tunnel System for Greenhouse Cooling, *Renewable Energy*, *35* (2010), 12, pp. 2804-2811
[24] Shahsavar, A., Rajabi, Y., Exergoeconomic and Enviroeconomic Study of an Air Based Building Integrated Photovoltaic/Thermal (BIPV/T) System, *Energy*, *144* (2018), Feb., pp. 877-886

Paper submitted: May 17, 2021
Paper revised: October 17, 2021
Paper accepted: April 29, 2022